

# Charge, density and electron temperature in a molecular ultracold plasma

C. J. Rennick, J. P. Morrison, J. Ortega-Arroyo, P. J. Godin and E. R. Grant  
*Department of Chemistry, University of British Columbia, Vancouver, BC V6T 1Z3, Canada*  
(Dated: April 16, 2022)

A Rydberg gas of NO entrained in a supersonic molecular beam releases electrons as it evolves to form an ultracold plasma. The size of this signal, compared with that extracted by the subsequent application of a pulsed electric field, determines the absolute magnitude of the plasma charge. This information, combined with the number density of ions, supports a simple thermochemical model that explains the evolution of the plasma to an ultracold electron temperature.

PACS numbers: 52.55.Dy, 32.80.Ee, 33.80.Gj, 34.80.Lx

Under suitable conditions, the quasi-neutral system of ions and electrons that forms an ultracold plasma can develop the properties of a strongly coupled fluid. This intriguing degree of charged-particle correlation occurs when the average interparticle Coulomb energy exceeds the thermal energy, or  $\Gamma > 1$ , where  $\Gamma$  quantifies the ratio of Coulomb to thermal energy in the ion and electron subsystem reservoirs:  $\Gamma_{i,e} = (q^2/4\pi\epsilon_0 a)/kT_{i,e}$ , in which the Wigner-Seitz radius,  $a$ , relates to the particle density by,  $\frac{4}{3}\pi a^3 = 1/\rho$ .

For  $\Gamma \approx 1$ , a plasma can form liquid-like correlations. Crystalline ordering sets in for  $\Gamma > 200$ . The creation of an ultracold plasma with these properties would provide an important laboratory analog for the strongly coupled systems that appear under extreme conditions at high temperatures and densities, such as in quark-gluon plasmas, at the centres of heavy stars and in the plasmas generated by the interaction of high-power lasers with solid targets.

Most often, ultracold plasma experiments start with a magneto-optical trap (MOT) in which an atomic gas sample with an initial temperature substantially lower than  $100 \mu\text{K}$  absorbs light from a high-resolution laser to release electrons with an average energy of  $10 \text{ K}$  or less [1]. In the plasma that forms, disorder induced heating and three-body electron-ion recombination drives electron and ion temperatures to values above the strongly coupled regime, typically  $T_i > 1 \text{ K}$  and  $T_e > 30 \text{ K}$ .

In a novel approach, we have excited nitric oxide cooled in a seeded supersonic beam to form a durable *molecular* ultracold plasma with an ion density exceeding  $1 \times 10^{12} \text{ cm}^{-3}$  [2], and an electron temperature, estimated from a Vlasov analysis, to fall with expansion from an initial value as low as  $7 \text{ K}$  to  $1 \text{ K}$  or less over a lifetime that extends beyond  $100 \mu\text{s}$  [3].

Such conditions of temperature and density suggest strong coupling parameters substantially greater than 1 for both ions and electrons. If confirmed, this degree of correlation would represent a significant milestone in ultracold plasma research. The molecular beam method offers a versatile means to study plasmas built both on atomic and a great many molecular precursors, and the well defined propagation of the plasma volume in the laboratory

frame presents significant advantages for imaging.

The present letter reports a measurement of the absolute excess charge of this plasma, and uses this information to construct a simple thermochemical model for its evolution from a Rydberg gas. This model serves to confirm our estimate of the total charged-particle density and suggest a mechanism by which this system attains such a low electron temperature. Calculations relate this feature directly to the high plasma densities achievable in a molecular beam.

Our experimental apparatus expands nitric oxide, seeded at 10% in helium, through a 0.5 mm diameter nozzle. A 1 mm diameter skimmer selects the core of this jet to form a molecular beam in the second stage of a differentially pumped electron spectrometer. Two frequency-doubled pulsed dye lasers intersect this beam 8 cm beyond the skimmer, between a pair of field grids, labeled  $G_1$  and  $G_2$  in Fig. 1. The first laser excites NO from its ground state to the  $v^+ = 0, N = 0$  level of the  $A(^2\Sigma^+)$  state. From this gateway state, the second dye laser drives the system of molecules to the  $n = 51, l = 3$  Rydberg state converging to the  $N^+ = 2$  rotational state of the ion ( $51f(2)$ ), which lies well below the lowest  $v^+ = 0, N^+ = 0$  ionization limit. At sufficient density, these Rydberg molecules interact, leading to a sequence of ionization processes that form an ultracold plasma [2].

This laser-crossed molecular beam illumination geometry creates a  $750 \mu\text{m}$  by c.a. 2 mm prolate ellipsoid excitation volume. The cross-beam density falls off rapidly along the long axis of this ellipsoid, and for convenience, we approximate the initial plasma density distribution as a  $750 \mu\text{m}$  diameter spherical Gaussian. Assuming saturated steps of double-resonant excitation, the density of NO at this point in the beam yields a molecular Rydberg density as high as  $5 \times 10^{12} \text{ cm}^{-3}$ , or a total of approximately  $10^9$  Rydberg-state NO molecules in the initial excitation volume.

We observe plasma formation heralded by a small signal of prompt electrons. A bias applied to  $G_1$  maintains a very weak field ( $-250 \text{ mV cm}^{-1}$ ) between  $G_1$  and  $G_2$ , which extracts these promptly released electrons for detection. Subsequently, the plasma moves with the velocity of the molecular beam toward the detector to reach

$G_2$ , which is grounded. On passing through this plane, the  $G_2$  grid extracts electrons, which accelerate in the  $100 \text{ V cm}^{-1}$  field between  $G_2$  and  $G_3$  to reach the detector. The resulting measured waveform represents the longitudinal electron density profile of the plasma.

A voltage pulse applied between  $G_1$  and  $G_2$ , before the plasma reaches  $G_2$ , serves as a probe to gauge the absolute magnitude of its excess positive charge. Using a Behlke high-voltage switch, we elevate  $G_1$  to a predetermined negative voltage for an interval of  $1 \mu\text{s}$ ,  $6 \mu\text{s}$  after the lasers have fired, which sends a pulse of extracted electrons to the detector. The grids return to near ground before the plasma passes through  $G_2$ .

Fig. 1 shows a waveform displaying the prompt signal of electrons associated with plasma formation, the electrons extracted from the plasma by the pulsed field applied as it travels between  $G_1$  and  $G_2$ , and the electrons shed as the plasma traverses the  $G_2$  grid. The prompt signal represents electrons released by Rydberg-Rydberg Penning ionization collisions, and by the subsequent electron impact ionization of Rydberg molecules. Electrons liberated by these processes escape the illuminated volume until the potential energy of the accumulating excess positive charge exceeds the average kinetic energy of the electrons that remain. Avalanche electron-impact ionization of bound Rydberg states continues [4], cooling these trapped electrons [5], until this process exhausts the population of Rydberg molecules.

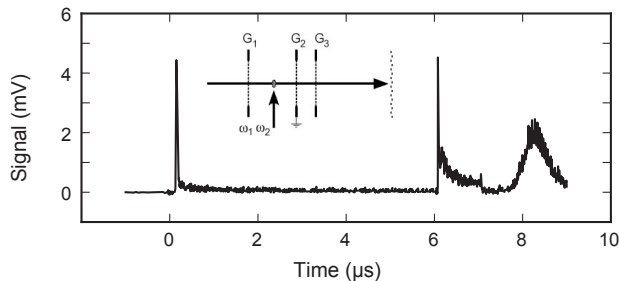


FIG. 1: Ultracold plasma electron signal waveform.  $75 \text{ V cm}^{-1}$  field applied between  $6$  and  $7 \mu\text{s}$ . Inset: Schematic diagram of the molecular beam flight path through a system of three grids to a microchannel plate detector.

We can estimate the total number of Rydberg molecules produced by photoexcitation [2]. The rate of plasma expansion gives a measure of the electron temperature as a function of time [3]. We see from the initial signal that prompt loss depletes the plasma of a certain number of electrons, producing a net positive space charge. It remains now to determine the absolute magnitude of this charge, and reconcile its appearance with the electron temperature evidenced by the rate of plasma expansion.

In relative terms, the prompt signal directly reflects the number of electrons lost to establish the plasma space

charge. Similarly, the pulsed-field extraction signal measures the number of electrons later extracted from this charged plasma by an electrostatic field of known absolute amplitude. Only one value of the absolute excess charge can produce a prompt signal and a set of pulsed-field extraction signals in the proportion we observe. Gauging the prompt signal against the signal extracted at each known pulsed-field amplitude, we can construct a self-consistent model by which to establish the absolute magnitude of the excess charge.

We treat our plasma as a charged, conductive Gaussian sphere. Applying an external field both tips the long-range potential and polarizes the plasma, adding a dipole component to the angular dependence of the potential at short range. A full description of these effects would require a self-consistent solution of the Poisson equation for the field-distorted electron density distribution, with the resulting calculated potential sensitive to the selected ion distribution [6]. We neglect this complexity, and instead regard the potential outside the plasma as that of a solid conductive sphere in an external field:

$$\phi(r, \theta) = \frac{Q}{4\pi\epsilon_0 r} - E_0 r \cos \theta + E_0 \frac{\sigma^3}{r^2} \cos \theta, \quad (1)$$

where  $\sigma$  is the radius of the sphere,  $Q$  is the total charge and  $E_0$  is the externally-applied field.

Electrons with a kinetic energy greater than the binding energy,  $\epsilon_{\text{crit}}$  leave the surface of the sphere with a flux dependent upon the distribution of velocity components normal to the surface element:

$$\frac{dN(\epsilon)}{dt} = \int_S \rho(\epsilon) v(\epsilon) r^2 \sin(\theta) d\phi d\theta. \quad (2)$$

Elastic collisions between the trapped electrons and ions transfer energy inefficiently owing to their large mass difference, so the ions remain at a low temperature. The electrons thermalize rapidly, however, on a timescale of a few plasma periods. We therefore assume that the electron kinetic energy distribution function is always Maxwellian. Thermalizing collisions fill-in the truncation that occurs as high kinetic-energy electrons from the tail of the distribution leave the plasma. While the electrons do not directly thermalize with the ions, the pressure of the trapped electrons causes the ion cloud to expand at a characteristic rate [7, 8, 9, 10]. We have measured the expansion rate of our plasma, and we estimate our electron temperature has cooled to  $6 \text{ K}$  when the pulsed field is applied [3].

We determine the electron flux leaving the spherical surface of our model plasma by integrating Eq. 2 over the electron energy distribution and the surface of our sphere numerically, calculating the integration limit  $\epsilon_{\text{crit}}$  dynamically at each time-step as the difference between the binding energy of an electron at the surface of the

plasma and the peak of the saddle-point using Eq. 1 with the charge given by the time-integrated electron flux,  $Q = Nq_e$ .

To simulate the experimental data, we select an initial plasma charge,  $Q_0$  and calculate the total number of electrons extracted at each applied field. Note that in each case, this model predicts an absolute number of electrons, while we measure integrated voltages that are only proportional to the collected charge. But, the same proportionality or detector efficiency also governs the prompt signal, which measures the electrons released to create  $Q_0$ . Thus, choosing a trial value of  $Q_0$  defines an operational detector efficiency. To fit the data, we vary  $Q_0$ , and calibrate the experimental signals accordingly for comparison with the predicted absolute yield of electrons extracted as a function of applied voltage. Figure 2 compares the data with simulations scaled in this way for three values of  $Q_0$ . A least-squares fit of the simulation to this data yields an estimated value of  $Q_0$  corresponding to the initial loss of  $1.17 \times 10^6$  electrons.

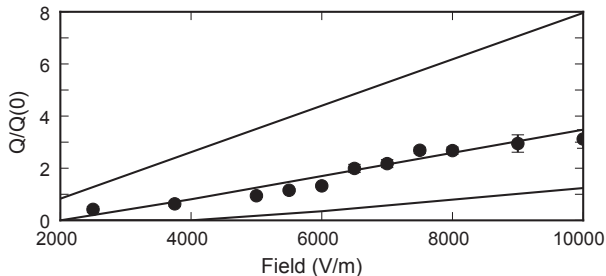


FIG. 2: Signal versus pulsed-field normalized by the plasma charge. Measured data (solid circles) normalized by the prompt signal. Calculated lines normalized by  $Q(0)$  chosen for the simulation. Line through the data points for an initial charge,  $N_i - N_e$ , of  $Q(0) = 1.17 \times 10^6$ . Upper and lower lines assume  $Q(0) = 0.58 \times 10^6$  and  $2.3 \times 10^6$  respectively.

A sequence of two events determines this excess charge and the observable electron temperature of the plasma. Penning collisions first convert pairs of NO Rydberg molecules into a free  $\text{NO}^+$  ion, an electron and a de-excited NO molecule, which very likely predissociates to form translationally excited neutral atoms. The excess energy of ionization creates an initial population of electrons with an average energy characterized by some temperature  $T'_e$ . This energy enables electrons to escape until the attractive potential of the developing  $\text{NO}^+$  space charge traps the electrons that remain. A cascade of collisions then excite and de-excite remaining NO Rydberg molecules, giving rise to an avalanche of electron-impact ionization events. Because these electron liberating collisions consume energy, the trapped electrons cool and remain confined [5, 11].

A few assumptions enable us to develop a simple model for this evolution to a plasma. Without loss of gener-

ality, we can regard the stages of Penning and electron-impact ionization to occur in sequence or overlap in time. The initial escape of Penning electrons evaporatively lowers  $T'_e$ , but we assume the loss of comparatively few confines the rest, making this effect negligible. During avalanche ionization, exothermic electron-Rydberg deactivating collisions can occur, but at early times this energy pooling process simply raises the phenomenological temperature of the Penning electrons. Unlike atoms, NO molecules in Rydberg states cascading to lower principal quantum number rapidly predissociate, and we assume that product N and O atoms leave the interaction volume without further affecting the electron or ion temperatures.

Experimentally, Killian et al.[12] found that they could describe the fraction of electrons trapped in various plasmas of defined excess energy as a uniform function of the number of ions  $N'_i$ , scaled by the threshold number,  $N^*$ , required in each case to trap electrons. This function, confirmed by simulations [13], relates  $N^*$  to the excess charge (the number of electrons lost) and  $N'_i$ , the number of ions (as produced in our case by Penning ionization):

$$N^* = \frac{(N'_i - N'_e)^2}{N'_i}. \quad (3)$$

$N^*$  increases for plasmas of higher electron temperature and larger radius,  $\sigma$ , as,

$$N^* = \frac{3}{2} k_B T'_e \sigma \frac{4\pi\epsilon_0}{q_e^2} \sqrt{\frac{\pi}{2}}. \quad (4)$$

where Eq. 4 expresses the threshold condition,  $N^*$ , as the ion density at  $T'_e$  for which  $\lambda_D \approx \sigma/2$ , where  $\lambda_D$  is the Debye length.

Our experiment measures the final excess charge,  $N_i - N_e$ , which we equate to  $N'_i - N'_e$ , on the assumption that no avalanche electrons escape. We can reasonably approximate the total number of Rydberg molecules, produced at saturation,  $N_0$ . We measure the electron temperature of the evolved plasma,  $T_e$  by determining its expansion rate.

Starting with  $N_i - N_e$ ,  $N_0$  and  $T_e$ , we can examine the energy balance for various trial values of  $N''_i$ , the number of ions formed by avalanche electron impact. Each trial value of  $N''_i$  produces an estimate of  $N'_i$ , calculated as.

$$N'_i = \frac{N_0 - N''_i}{2}. \quad (5)$$

From this value of  $N'_i$ , we obtain  $N^*$  from Eq. 3. We can then use Eq. 4 to determine a temperature  $T'_e$  of the Penning electrons.

Each ion produced by electron impact ionization of a nitric oxide molecule in the  $51f(2)$  Rydberg state consumes the binding energy  $\Delta E_n = 8.38 \times 10^{-22}$  J. Thus,

avalanche ionization to form  $N_i''$  ions lowers the electron temperature of the plasma to a value,  $T_e$ , such that:

$$T_e = \frac{\frac{3}{2}k_B T_e' N_i' - N_i'' \Delta E_n}{\frac{3}{2}k_B (N_i' + N_i'')} . \quad (6)$$

Using Eqs. 3 – 5, we can write  $T_e$  in terms of the measured charge,  $N_i - N_e$ , and the fraction,  $f$ , of Rydberg NO molecules ionized by avalanche electron impact.

$$T_e = \frac{q_e^2 (N_i - N_e)^2 / \sqrt{\pi} \sigma 4 \pi \epsilon_0 - f N_0 \Delta E_n}{\frac{3}{2} k_B N_0 (f + 1) / 2} . \quad (7)$$

Figure 3 shows values of  $T_e$  predicted by Eq. 7 as a function of  $f$  for assumed values of  $N_0$ , decreasing from a saturated  $N_0 = 1.1 \times 10^9$  (density,  $n_e = 5 \times 10^{12} \text{ cm}^{-3}$ ).

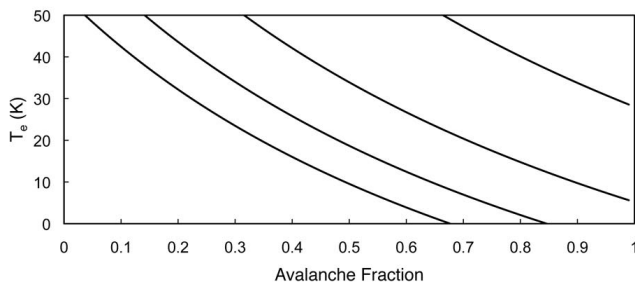


FIG. 3: Evolved plasma temperature predicted from thermochemical energy balance as a function of avalanche fraction,  $f$ , for assumed values of initial Rydberg density,  $N_0$ , reading from the left, of  $5, 4, 3$  and  $2 \times 10^{12} \text{ cm}^{-3}$ .

This variation in plasma electron temperature reflects the simple thermochemical balance in which electron heating, manifested in the observed excess charge, dissipates in the cooling necessary to complete avalanche ionization. The high characteristic frequency of electron motion compared with that of Penning collisions surely causes avalanche ionization to dominate soon after enough electrons escape to establish a trapping potential, favouring  $f \approx 1$ . As the electrons cool, energy transferred per collision must eventually drop to the point that Rydberg predissociation overtakes ionization and cooling stops. This condition leads simply to a thermochemical balance for some smaller effective value of  $N_0$ .

Thus, for an assumed avalanche fraction of 95 percent, the conversion of an effective Rydberg density of  $3.0 \times 10^{12} \text{ cm}^{-3}$  ( $N_0 = 6.6 \times 10^8$ ) forms a plasma with an electron temperature of  $T_e = 7 \text{ K}$ . Initial Penning collisions produce the  $N_i' = 1.6 \times 10^7$   $\text{NO}^+$  ions called for by Eq. 5, which release an excess charge conforming with the measured value of  $1.1 \times 10^6$  electrons from an energy distribution with a temperature of  $T_e' = 1850 \text{ K}$ .

This simple model neglects some obvious aspects of the plasma evolution dynamics. For example, as mentioned above it considers neither the reduction in  $T_e'$  that

occurs as a consequence of early electron escape, nor increase in  $T_e$  by electron-impact deactivation of NO Rydberg states. However, we know that the plasma loses comparatively few hot electrons to form its trapping potential, and we can assume that collisional deactivation of Rydberg NO accelerates predissociation, which rapidly depletes the plasma of molecules in quantum states below the bottleneck for collisional ionization [14, 15].

Regardless of its simplifying assumptions, this crude energy balance does serve to show that a feasible route exists for the molecular plasma of  $\text{NO}^+$  ions and electrons formed in a molecular beam to reach a low electron temperature. The variation in the cooling range with  $N_0$  shows clearly how high density plays a critical role in providing a sufficient reservoir of Rydberg bound states to cool the system as it evolves. Fortunately, typical conditions attained in pulsed dye laser crossed differentially pumped molecular beams yield excited state densities in this range for many molecular systems.

The authors gratefully acknowledge helpful discussions with Thomas Pohl. This work was supported by NSERC, the Canada Foundation for Innovation (CFI) and the BC Knowledge Development Fund (BCKDF).

- 
- [1] T. Killian, T. Pattard, T. Pohl, and J. Rost, *Physics Reports* **449**, 77 (2007).
  - [2] J. P. Morrison, C. J. Rennick, J. S. Keller, and E. R. Grant, *Phys. Rev. Lett.* **101**, 205005 (2008).
  - [3] J. P. Morrison, C. J. Rennick, and E. R. Grant, *Phys. Rev. A* **79**, 062706 (2009).
  - [4] T. Pohl, T. Pattard, and J. M. Rost, *Phys. Rev. A* **68**, 010703(R) (2003).
  - [5] T. Pohl, D. Comparat, N. Zahzam, T. Vogt, P. Pillet, and T. Pattard, *Eur. Phys. J. D* **40**, 45 (2006).
  - [6] D. Vrinceanu, G. Balaraman, and L. Collins, *J. Phys. A* **41**, 425501 (2008).
  - [7] S. Laha, P. Gupta, C. E. Simien, H. Gao, J. Castro, T. Pohl, and T. C. Killian, *Phys. Rev. Lett.* **99**, 155001 (2007).
  - [8] P. Gupta, S. Laha, C. E. Simien, H. Gao, J. Castro, T. C. Killian, and T. Pohl, *Phys. Rev. Lett.* **99**, 075005 (2007).
  - [9] E. Cummings, J. Daily, D. Durfee, and S. Bergeson, *Phys. Plasmas* **12** (2005).
  - [10] F. Robicheaux and J. D. Hanson, *Phys. Plasmas* **10**, 2217 (2003).
  - [11] N. Vanhaecke, D. Comparat, D. A. Tate, and P. Pillet, *Phys. Rev. A* **71**, 013416 (2005).
  - [12] T. C. Killian, S. Kulin, S. D. Bergeson, L. A. Orozco, C. Orzel, and S. L. Rolston, *Phys. Rev. Lett.* **83**, 4776 (1999).
  - [13] D. Comparat, T. Vogt, N. Zahzam, M. Mudrich, and P. Pillet, *Mon. Not. R. Astron. Soc.* **361**, 1227 (2005).
  - [14] S. G. Kuzmin and T. M. O'Neil, *Phys. Plasmas* **9**, 3743 (2002).
  - [15] P. Mansbach and J. Keck, *Phys. Rev.* **181**, 275 (1969).